Nano Research
DOI 10.1007/s12274-016-1219-2
Research Article
ISSN 1998-0124
CN 11-5974/O4

A carbon nanofiber network for stable lithium metal anodes with high Coulombic efficiency and long cycle life

Anyi Zhang[1], Xin Fang[1], Chenfei Shen[1], Yihang Liu[2], and Chongwu Zhou[1,2] (✉)

[1] *Mork Family Department of Chemical Engineering and Materials Science, University of Southern California, Los Angeles 90089, USA*
[2] *Ming Hsieh Department of Electrical Engineering, University of Southern California, Los Angeles 90089, USA*

Received: 10 February 2016
Revised: 15 July 2016
Accepted: 17 July 2016

KEYWORDS
lithium-ion batteries, lithium metal anode, carbon nanofiber, three-dimensional conductive network

ABSTRACT

Li metal is considered one of the most promising candidates for the anode material in high-energy-density Li-ion batteries. However, the dendritic growth of Li metal during the plating/stripping process can severely reduce Coulombic efficiency and cause safety problems, which is a key issue limiting the application of Li metal anodes. Herein, we present a novel strategy for dendrite-free deposition of Li by modifying the Cu current collector with a three-dimensional carbon nanofiber (CNF) network. Owing to the large surface area and high conductivity of the CNF network, Li metal is inserted into and deposited onto the CNF directly, and no dendritic Li metal is observed, leaving a flat Li metal surface. With Li metal as the counter electrode for Li deposition, an average Coulombic efficiency of 99.9% was achieved for more than 300 cycles, at large current densities of 1.0 and 2.0 mA·cm^{-2}, and with a high Li loading of 1 mAh·cm^{-2}. The scalability of the preparation method and the impressive results achieved here demonstrate the potential for the application of our design to the future development of dendrite-free Li metal anodes.

1 Introduction

Since Sony commercialized lithium-ion rechargeable batteries in 1991, graphite has been used as the anode material. With the increasing demand for batteries for electronic devices and electrical vehicles, the limitations of the specific capacity of both the cathode and anode materials has become the bottleneck to the improvement of battery performance. Li metal anodes have attracted much interest due to their relatively high specific capacity (3,860 mAh·g^{-1}), low density (0.534 g·cm^{-3}), and low electrochemical potential (−3.04 V vs. standard hydrogen electrode). In addition, Li metal can be matched with promising Li-free cathode materials, such as sulfur [1–3], O_2 [4, 5], and V_2O_5 [6, 7], to achieve high-energy-density batteries.

Li metal has been well studied as an anode material since Li batteries were first proposed in the 1970s [8, 9]. However, the formation of Li dendrites, which leads to safety issues and low Coulombic efficiency, has

Address correspondence to chongwuz@usc.edu

limited the commercialization of Li metal anodes [10]. The phenomenon of Li dendritic growth was first observed in the 1960s, but the mechanism is complicated and still not well understood [11–13]. A popular model to explain this phenomenon suggests that the ramified growth of Li is mainly caused by the non-uniformity of charge distribution on the Li surface [14, 15]. Li metal can react with organic solvents and Li salts in the electrolyte to form a solid electrolyte interface (SEI) layer [16], which is ionically conductive but electrically insulating. However, the thickness of the SEI layer is not uniform throughout the surface owing to localized ion concentration gradients, resulting in different ion conductivity. In addition, the volume change of the Li metal during the Li plating/stripping process can crack the SEI layer and expose the Li to the electrolyte. Finally, the Li metal underneath a thinner or cracked SEI layer can grow faster than the other parts, resulting in the dendritic growth of the Li metal.

A great deal of research effort has been dedicated to resolving the problem of dendrite formation. Generally speaking, three strategies have been proposed: (1) modifying the electrolyte to obtain a stable SEI; (2) adding a stable interlayer to physically trap Li dendrites; and (3) introducing a network to form a three-dimensional (3D) structure for uniform Li deposition. Based on the first strategy, Qian et al. [17] reported that the use of highly concentrated electrolytes (4 M) composed of 1,2-dimethoxyethane (DME) and lithium bis(fluorosulfonyl)imide (LIFSI) salt can suppress dendrite growth. In addition, some additives in electrolytes, e.g., trace amounts of water (H_2O), have also been reported to affect the surface morphology [18]. However, using a highly concentrated electrolyte can increase the total cost significantly, and introducing certain additives can result in side reactions with the cathode materials. Besides changing the electrolyte components, adding a chemically stable and mechanically strong interlayer between the Li anodes and electrolytes is another alternative approach to stabilizing the SEI layer. Zheng et al. [19] used interconnected hollow carbon nanospheres as interlayers to stabilize the interface between the Li and electrolytes. Furthermore, Yan et al. [20] demonstrated that two-dimensional atomic crystals (single-layer boron nitride (h-BN) and graphene) can also work as interlayers to prevent the growth of Li dendrites. In addition to adding interlayers directly onto the Li metal surface, Luo et al. [21] coated separators with BN to form thermally conductive separators. They found that a homogeneous thermal distribution was important for uniform Li deposition. Improved Coulombic efficiencies have been demonstrated with this strategy. However, the amount of Li deposited underneath was limited, since the two-dimensional (2D) interlayer cannot accommodate the large volume variation during the plating/stripping process. The use of 3D structures is proposed as an ideal approach to address this problem [22–24]. Liang et al. [25] utilized oxidized polyacrylonitrile (PAN) nanofibers on top of current collectors to modify the Li metal anode and form flat surfaces. Because of the insulating nature of PAN, the 3D structure introduced in this method can only work as a scaffold to guide the growth of the Li metal. Besides insulating networks like PAN, Cheng et al. [26] used a conductive graphene framework for Li deposition and successfully improved Coulombic efficiencies to around 97% for more than 100 cycles. Different from an insulating network, a conductive network can provide a large surface area for Li deposition so that areal current densities can be lessened significantly, which is beneficial for uniform current distribution.

In our opinion, a promising 3D network for Li deposition should have three features: (1) good conductivity, which allows Li to deposit onto the surface of the network and lowers the impedance of the electrode; (2) large surface area, which can reduce the areal current density; and (3) good flexibility and sturdiness, which can accommodate the large volumetric change in the Li metal during the plating/stripping process. According to this strategy, we propose a carbon nanofiber (CNF) network for stable Li metal anodes, since CNF films produced by vacuum filtration can achieve the three aforementioned features simultaneously. The graphitic structure of CNFs can also provide many active sites for Li ion insertion, leading to uniform Li deposition throughout the 3D structure. In addition, the compound SEI layer formed during cycling, which has been characterized by X-ray photoelectron spectroscopy (XPS), can further protect

the surface of Li metal anodes. In this paper, we demonstrate that Cu foil current collectors modified with CNF films can improve the Coulombic efficiency of the Li plating/stripping process to 99.9% for 300 cycles at a current density of 1.0 and 2.0 mA·cm^{-2}, which is among the best performance reported to date in terms of both Coulombic efficiency and cyclability.

2 Experimental

2.1 Carbon nanofiber film preparation

The CNF material we used was PR-24-XT-HHT from Pyrograf Products, which was fully graphitized by a 3,000 ℃ procedure for high conductivity and has a specific surface area as large as 41 m^2·g^{-1}. CNF films were prepared by a simple vacuum filtration method. Before filtration, the CNF material was washed in a mixture of HNO_3 and H_2SO_4 to make it hydrophilic. The volumetric ratio of HNO_3 to H_2SO_4 was 2:1. In the acid treatment, 200 mg CNFs were well mixed with 15 mL acid solution and heated to 90 ℃ for 10 h. The mixture was then diluted with 1.0 L deionized water and filtered to obtain acid-washed CNFs. To make our desired CNF film, 20 mg acid-washed CNFs were well dispersed in 20 mL ethanol and vacuum filtered. After drying, a CNF film can be peeled off from the filtration paper easily and punched into 1.5 cm^2 pieces. The total mass of each CNF piece was 2.8 mg.

2.2 Electrochemical testing

For electrochemical measurement, CR2032 coin cells were assembled using Li foils as the counter electrode. To make our modified electrode, a Cu current collector was coated with a thin layer of 5% polyvinylidene fluoride (PVDF) solution in N-methyl pyrrolidone (NMP). Then, a small piece of CNF film was adhered to the Cu current collector, which was then used as a modified electrode for Li deposition. Pristine Cu current collectors were also tested as control electrodes. The electrolyte was lithium bis(trifluoromethanesulfonyl)imide (LITFSI) in 1,2-dimethoxyethane (DME) and 1,3-dioxolane (DOL) (volume ratio 1:1) with a 0.5 M lithium nitrate ($LiNO_3$) additive. Cycling tests were carried out by discharging at 1.0 mA·cm^{-2} for 1 h and then charging to 1.0 V at the same current density. For the cycling tests with a higher current rate, the batteries were discharged at 2.0 mA·cm^{-2} for 30 min and charged to 1.0 V at 2.0 mA·cm^{-2}. To exclude the capacity from the CNF material itself, the modified electrode was also tested with a potential window from 0.01 to 1.0 V as a control sample. Electrochemical impedance spectroscopy (EIS) measurement was performed after the 50th discharge at 1.0 mA·cm^{-2} on a Gamry electrochemical workstation.

2.3 Characterization

The morphology of the electrodes was characterized using a JEOL JSM-7001 scanning electron microscope (SEM) operated at 10 kV. Samples after cycling were washed with DME to remove the electrolyte residue and dried in an argon-filled glovebox. X-ray photoelectron spectroscopy (XPS) was conducted using a Kratos AXIS Ultra. To exclude the effect of the electrolyte, control samples were made by immersing the CNF films into electrolyte without Li deposition, where all other processes were conducted under the same conditions.

3 Results and discussion

We developed a simple method to stabilize Li metal anodes with a CNF network. The role CNF plays in Li metal deposition process is illustrated schematically in Fig. 1, in comparison with a pristine Cu current collector. During the plating/stripping process, a Li dendrite can be formed on the Cu, as shown in Fig. 1(a), leading to degradation of the Coulombic efficiency. More importantly, the dendritic growth of the Li can result in a short circuit, causing serious safety concerns. With a CNF film on top of the Cu current collector, as shown in Fig. 1(b), the surface area increases significantly, providing an ideal conductive network for Li deposition. During the plating/stripping processes, Li ions are deposited onto the surface of the CNFs, preventing the formation of Li dendrites.

SEM was used to characterize the morphology of electrodes before and after cycling for both modified and control samples. When Li metal is deposited onto pristine Cu foil at a current density of 1.0 mA·cm^{-2} for 1 h, the formation of Li dendrite is observed after 50 cycles, as shown in Figs. 2(a) and 2(b). The top

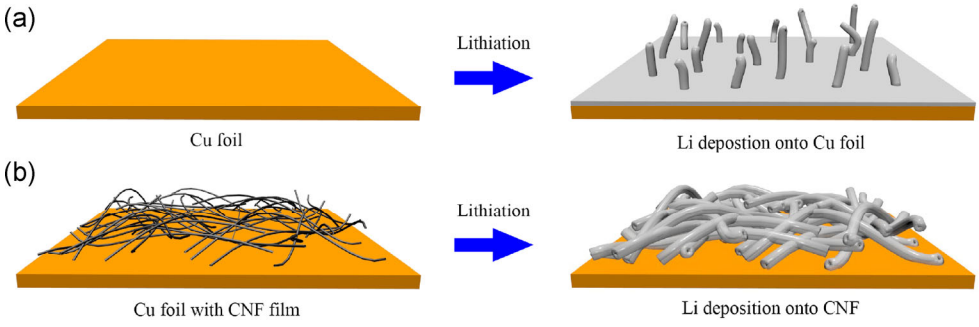

Figure 1 Schematic of Li deposition on (a) pristine Cu foil and (b) Cu foil with CNF modification.

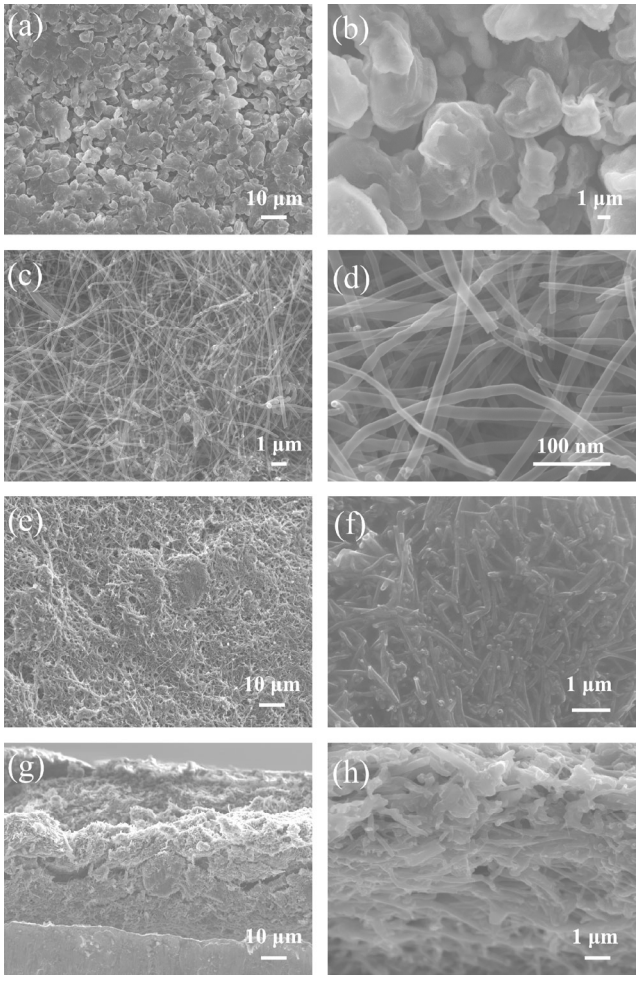

Figure 2 SEM images of the morphologies of ((a) and (b)) Li deposition onto pristine Cu foil, ((c) and (d)) pristine CNF network, ((e) and (f)) top view of Li deposition on a CNF network, and ((g) and (h)) cross section of Li deposition on a CNF network.

surface of the deposited Li presents a very uneven structure. The morphology of a pristine CNF film is shown in Figs. 2(c) and 2(d). The CNFs have a hollow structure with a diameter of ca. 10–20 nm. This CNF network provides enough void space for Li deposition and can tolerate the volumetric variation of the Li metal during the plating/stripping process. Figures 2(e) and 2(f) show the top view of a CNF electrode after the 50th discharge process. Owing to the conductive CNF network, the surface of the deposited Li metal is very flat and no dendritic Li growth is observed. CNFs work as a framework to support the Li metal and as a built-in current collector to improve the uniformity of current density distribution. To investigate the spatial distribution of the Li, images showing the cross-section of CNF electrodes after Li deposition are presented in Figs. 2(g) and 2(h). Li was deposited onto both the top and the bottom sides of CNF network homogeneously, confirming the spatial uniformity of Li deposition. Compared with 2D Cu foils, the 3D structure provides an enormous surface area for Li deposition. Since Li ions can diffuse inside the CNF network, Li can deposit onto the CNFs throughout the 3D structure, which can reduce the areal current density significantly. In this way, Li metal is trapped inside the 3D CNF network without any dendritic Li growth, and safety issues caused by short circuits can be avoided.

To study the electrochemical performance of the CNF-modified Li anodes, coin cells were assembled with Li foils as counter electrodes. Pristine Cu foils were used as control samples to demonstrate the effect of the CNF layer. The coin cells were discharged for a constant time and charged to a constant voltage in each cycle. In this way, the Coulombic efficiency, which is defined as the ratio of the Li capacity during the charge process versus the Li capacity during the discharge process, can be used as an important parameter to determine the reversibility of the Li deposition. Figure 3(a) illustrates the Coulombic

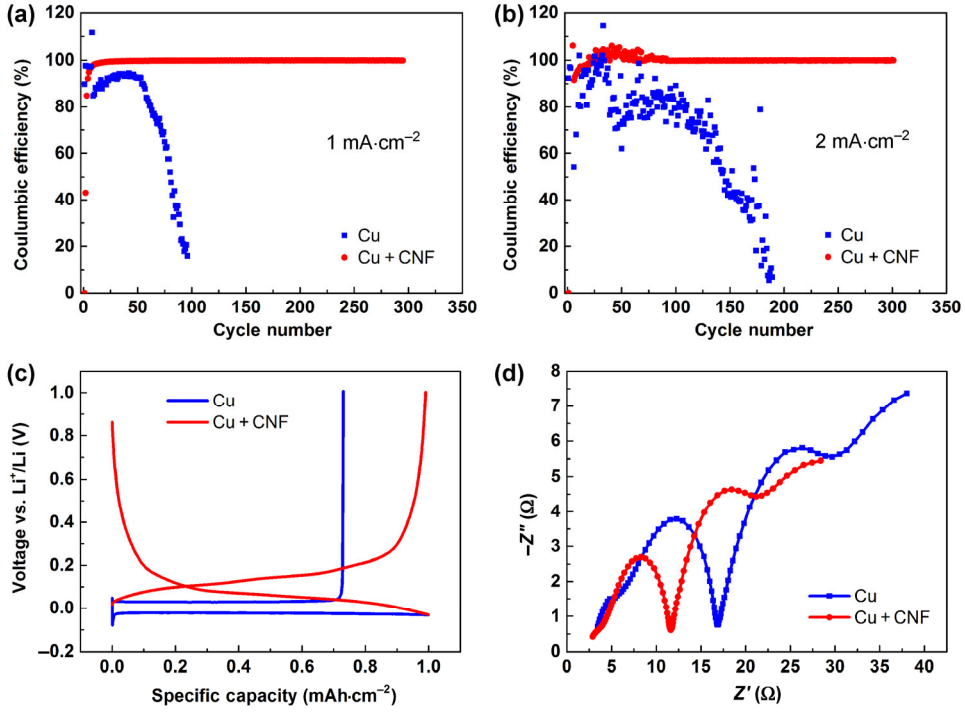

Figure 3 Electrochemical performances of Cu and Cu + CNF electrodes. (a) Comparison of the Coulombic efficiency of Li deposition on Cu and Cu + CNF electrodes at a current density of 1.0 mA·cm^{-2}. The amount of Li deposited in each cycle is 1.0 mAh·cm^{-2}. (b) Comparison of the Coulombic efficiency of Li deposition on Cu and Cu + CNF electrodes at a current density of 2.0 mA·cm^{-2}. The amount of Li deposited in each cycle is 0.5 mAh·cm^{-2}. (c) Comparison of the voltage profiles of the 60th Li plating/stripping process on Cu and Cu + CNF electrodes with a current density of 1.0 mA·cm^{-2}. (d) Nyquist plots of the Cu and Cu + CNF electrodes after the 50th plating process.

efficiencies of both CNF-modified electrodes (designated Cu + CNF) and pristine Cu electrodes (designated Cu) at a current density of 1.0 mA·cm^{-2} with a discharging time of 1 h. The low Coulombic efficiencies of both electrodes in the first several cycles can be attributed to the formation of SEI layers. After ca. 10 cycles, the Coulombic efficiency of the Cu + CNF electrode increases to more than 98%. After 100 cycles, the Coulombic efficiency reaches ca. 99.9% and remains at this level up to 300 cycles. However, the Coulombic efficiency of the control sample begins to degrade after 50 cycles and drops to less than 20% after 100 cycles. Similar trends are observed at higher current densities. At 2.0 mA·cm^{-2}, as shown in Fig. 3(b), the Coulombic efficiency of the Cu + CNF electrode remains at ca. 99.9% after 300 cycles and the Coulombic efficiency of the Cu electrode drops to less than 10% over 200 cycles. Thus, the reversibility of the Li plating/stripping process is improved significantly by CNF modification. The voltage profiles of both modified and control electrodes in the 60th cycle are shown in Fig. 3(c). It is interesting to note that the voltage profile of the modified electrode is quite different from that of the control electrode. With pristine Cu, the voltage plateau is very flat. However, with the introduction of CNFs, a slight slope can be observed, suggesting that CNFs contribute a small amount of capacity to the total capacity. The discharge/charge curves of a modified electrode up to 100 cycles are plotted in Fig. S1 in the Electronic Supplementary Material (ESM). Starting from the 2nd cycle, the voltage plateaus for both samples become stable and show similar curve features as those observed for the 60th cycle. In fact, CNFs have been studied as an anode material for Li-ion batteries [27, 28] and Li ions can also insert into the graphitic structure of CNFs. In this way, the Li plating process can be separated into two steps with different mechanisms. With decreasing voltage, Li ions are first inserted into the CNFs, resulting in a slope in the voltage profile. Then, Li ions begin to

deposit onto the surface of the CNFs as the insertion of Li ions approaches saturation. The voltage decreases to below 0 V during this step, further confirming that Li deposits directly onto the surface. To exclude the specific capacity of the CNFs, we tested the CNFs as a regular anode material with a potential window from 0.01 to 1.0 V, as shown in Fig. S2 in the ESM. Obviously, the gravimetric specific capacity of our modified Li metal anode (536 $mAh \cdot g^{-1}$) is much higher than the internal specific capacity of the CNFs (220 $mAh \cdot g^{-1}$) and even the theoretical specific capacity of graphite (372 $mAh \cdot g^{-1}$). To characterize the resistances for both the modified and control electrodes, the EIS analysis was performed after the 50th discharge process, as shown in Fig. 3(d). An equivalent circuit was used to interpret the Nyquist plots (Fig. S3 in the ESM) and the calculated results are shown in Table 1. Both Cu + CNF and Cu electrodes exhibit a similar R_{Ω}, which corresponds to resistances from the electrodes and the electrolyte. However, the Cu + CNF electrode presents much lower R_{SEI} and R_{CT} values. R_{SEI} represents the resistance from the SEI layer, while R_{CT} represents the resistance from charge transfer. The low resistance of the Cu + CNF electrode helps to distribute the current homogeneously, resulting in uniform Li deposition over the whole surface area.

In order to investigate how the flat surface of Li metal is formed, SEM images were taken after the 1st, 5th, and 10th discharge and charge cycles, which are shown in Fig. 4 and Fig. S4 in the ESM. The different morphologies of the Li metal surfaces after different numbers of cycles can be clearly observed. After the 1st discharge process (Fig. 4(a)), Li is deposited onto CNFs directly, leaving some void space inside the CNF network. Compared with pristine Cu foil, the CNF network increases the active surface area for Li deposition tremendously so that the areal current density is reduced dramatically. Most of the Li metal is stripped after the 1st charge process (Fig. 4(b));

Table 1 Comparison of R_{Ω}, R_{SEI}, and R_{CT} for both Cu and Cu + CNF electrodes

	R_{Ω} (Ω)	R_{SEI} (Ω)	R_{CT} (Ω)
Cu + CNF	2.873	9.837	4.724
Cu	2.803	15.44	10.53

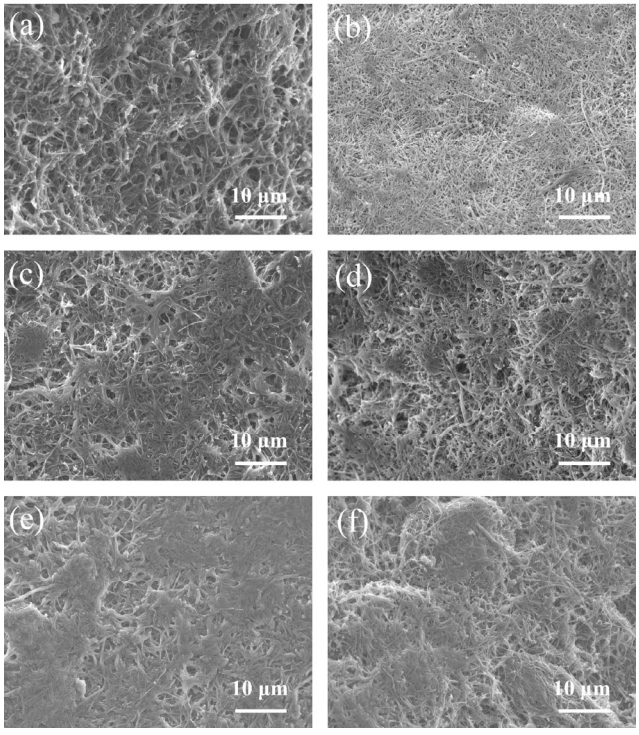

Figure 4 SEM images showing the morphologies of Cu + CNF electrodes after (a) the 1st plating process, (b) the 1st stripping process, (c) the 5th plating process, (d) the 5th stripping process, (e) the 10th plating process, and (f) the 10th stripping process.

however, some residue is left on the CNFs. We suspect that the residue mainly comes from the SEI layer, which could not be stripped during the charge process. After the 5th discharge (Fig. 4(c)) and charge (Fig. 4(d)) process, more residue is observed on the CNFs, and some of it has coalesced. After 10 cycles, some terraces with flat surfaces can be observed due to the expansion of the residue. Since the SEI layer is electrically insulating and ionically conductive, Li can still be plated underneath the flat surface, but no Li dendrite can be formed on top of it. In this way, the SEI layer works as a stable cap to suppress the growth of Li dendrites.

To further understand the chemical composition of the SEI layer, Cu + CNF electrodes after cycling were rinsed with DME and analyzed by XPS. The C 1s, O 1s, F 1s, and N 1s spectra are provided in Fig. 5. In order to exclude the influence of the CNFs and electrolyte, a pristine Cu + CNF electrode, which was first immersed in electrolyte and then rinsed with DME, was tested as a control sample. We compared the survey spectra of the Cu + CNF electrodes after

cycling and before cycling, as shown in Fig. S5 in the ESM. Obviously, no F 1s, N 1s, S 2p, or Li 1s peaks are observed before cycling, confirming the complete removal of the electrolyte by DME. In this regard, all the peaks in Fig. 5 are confirmed to result from SEI and the CNFs, rather than the electrolyte. The C 1s spectrum of the Cu + CNF electrode after cycling, which is plotted in Fig. 5(a), can be separated into four peaks (284.2, 285.3, 287.0, and 289.5 eV). These peaks can be assigned to graphitic carbon, C–C (or C–H), C–O, and O–(C=O) –O, respectively [29–32]. In Fig. 5(b), typical C–O and C=O oxygen peaks are presented at 534.1 and 532.1 eV, respectively [33]. However, the O 1s peak for C=O is quite dominant compared with the peak for C–O. Based on the C 1s and O 1s spectra, we believe that the SEI contains a large amount of $LiCO_3$ and/or lithium alkyl carbonates ($ROCO_2Li$). These carbonate species are formed by the electrochemical reduction of organic solvents (DOL and DME), which is widely reported for various electrolyte systems [30, 34–36]. For the F 1s spectrum (Fig. 5(c)), peaks at 688.9 and 685.0 eV can be attributed to CF_3 and F^-, respectively [37]. This indicates that the SEI layer also contains LiF, which is a typical product of LiTFSI decomposition on the surface of Li metal. $LiNO_3$ (0.5 M) was added to our electrolyte as an additive to further protect the Li metal anode. In Fig. 5(d), the N 1s spectrum can be separated into three peaks (404.4, 401.2, and 399.3 eV) assigned respectively to $LiNO_2$, $Li_2N_2O_2$, and Li_3N [38, 39]. These species result from the reduction of $LiNO_3$, as reported in the literature. The SEI layer with complex components provides a strong surface film and further improves the stability of the Li metal anode.

4 Conclusions

In conclusion, we have demonstrated the utility of CNF-modified Cu current collectors as Li metal anodes. At current densities of 1.0 and 2.0 $mA \cdot cm^{-2}$, the Li metal anode with CNF modification can be cycled for more than 300 cycles with a specific capacity of 1.0 $mAh \cdot cm^{-2}$ and a stable Coulombic efficiency of ca. 99.9%. This excellent performance is attributed to the high conductivity and large specific surface area of the CNF network and the internal capacity of the

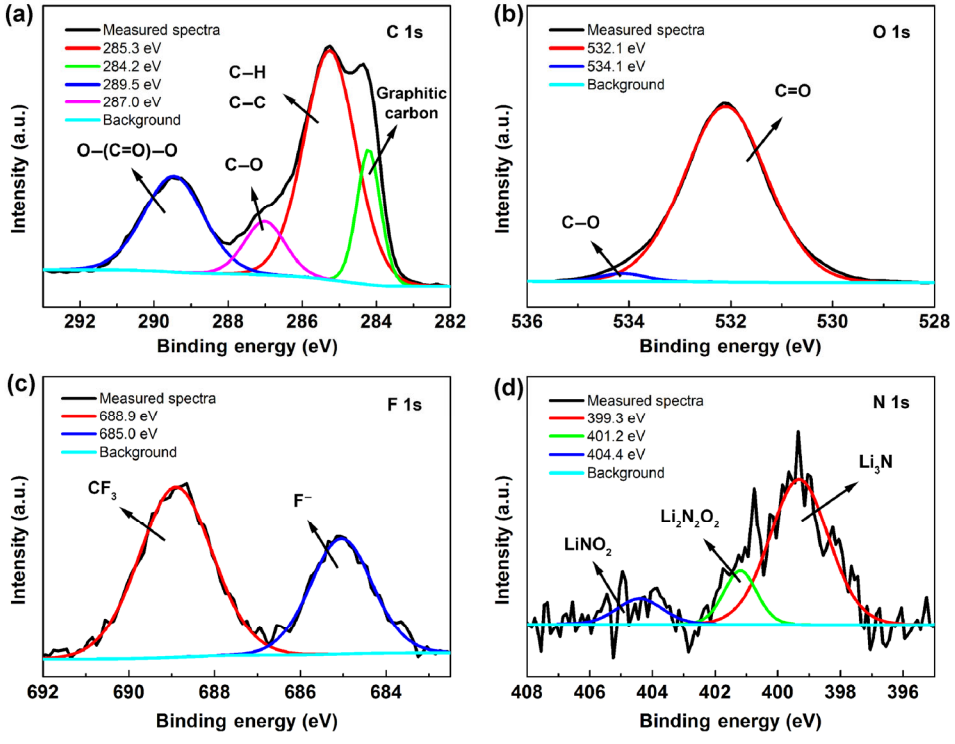

Figure 5 XPS spectra for the (a) C 1s regions, (b) O 1s regions, (c) F 1s regions, and (d) N 1s regions of Cu + CNF electrodes after cycling.

CNFs. The 3D structure provides abundant reaction sites for Li insertion and plentiful void space for Li deposition. In this way, areal current densities are reduced and distributed uniformly throughout the total structure, leading to even Li growth without the formation of dendrites. Furthermore, a stable SEI layer with a complex composition can be formed during cycling, and protects the Li metal anode as a strong coating film. Further research is ongoing to increase the Coulombic efficiencies in the first several cycles, which is an important issue for practical application. In addition, the integration of a limited Li source with various cathode materials is also challenging. We believe that Li metal anodes with effective modifications will become promising candidates as anode materials for next-generation high-energy-density Li-ion batteries.

Acknowledgements

A portion of the images and data used in this article were generated at the Center for Electron Microscopy and Microanalysis, University of Southern California. The EIS data used in this article was collected in Dr. Stephen Cronin's lab.

Electronic Supplementary Material: Supplementary material (the voltage profiles of Li plating/stripping process on a Cu + CNF electrode, electrochemical performance of CNF tested as anode, simulated Nyquist plots of Cu and Cu + CNF electrodes, high magnification SEM images of Cu + CNF electrodes after Li plating/stripping processes, XPS survey spectra for the Cu + CNF electrodes) is available in the online version of this article at http://dx.doi.org/10.1007/s12274-016-1219-2.

References

[1] Shen, C. F.; Ge, M. Y.; Zhang, A. Y.; Fang, X.; Liu, Y. H.; Rong, J. P.; Zhou, C. W. Silicon(lithiated)–sulfur full cells with porous silicon anode shielded by Nafion against polysulfides to achieve high capacity and energy density. *Nano Energy* **2016**, *19*, 68–77.

[2] Ji, X. L.; Lee, K. T.; Nazar, L. F. A highly ordered nanostructured carbon–sulphur cathode for lithium–sulphur batteries. *Nat. Mater.* **2009**, *8*, 500–506.

[3] Chen, S. Q.; Sun, B.; Xie, X. Q.; Mondal, A. K.; Huang, X. D.; Wang, G. X. Multi-chambered micro/mesoporous carbon nanocubes as new polysulfides reserviors for lithium–sulfur batteries with long cycle life. *Nano Energy* **2015**, *16*, 268–280.

[4] Girishkumar, G.; McCloskey, B.; Luntz, A. C.; Swanson, S.; Wilcke, W. Lithium–air battery: Promise and challenges. *J. Phys. Chem. Lett.* **2010**, *1*, 2193–2203.

[5] Wang, J. J.; Li, Y. L.; Sun, X. L. Challenges and opportunities of nanostructured materials for aprotic rechargeable lithium–air batteries. *Nano Energy* **2013**, *2*, 443–467.

[6] Cao, A. M.; Hu, J. S.; Liang, H. P.; Wan, L. J. Self-assembled vanadium pentoxide (V_2O_5) hollow microspheres from nanorods and their application in lithium-ion batteries. *Angew. Chem., Int. Ed.* **2005**, *44*, 4391–4395.

[7] Liang, S. Q.; Hu, Y.; Nie, Z. W.; Huang, H.; Chen, T.; Pan, A. Q.; Cao, G. Z. Template-free synthesis of ultra-large V_2O_5 nanosheets with exceptional small thickness for high-performance lithium-ion batteries. *Nano Energy* **2015**, *13*, 58–66.

[8] Rao, B. M. L.; Francis, R. W.; Christopher, H. A. Lithium-aluminum electrode. *J. Electrochem. Soc.* **1977**, *124*, 1490–1492.

[9] Kanamura, K.; Tamura, H; Shiraishi, S; Takehara, Z. Morphology and chemical compositions of surface films of lithium deposited on a Ni substrate in nonaqueous electrolytes. *J. Electroanal. Chem.* **1995**, *394*, 49–62.

[10] Aurbach, D.; Zinigrad, E.; Teller, H.; Dan, P. Factors which limit the cycle life of rechargeable lithium (metal) batteries. *J. Electrochem. Soc.* **2000**, *147*, 1274–1279.

[11] Kominato, A.; Yasukawa, E.; Sato, N.; Ijuuin, T.; Asahina, H.; Mori, S. Analysis of surface films on lithium in various organic electrolytes. *J. Power Sources* **1997**, *68*, 471–475.

[12] Brissot, C.; Rosso, M.; Chazalviel, J.-N.; Lascaud, S. Dendritic growth mechanisms in lithium-polymer cells. *J. Power Sources* **1999**, *81–82*, 925–929.

[13] Harry, K. J.; Hallinan, D. T.; Parkinson, D. Y.; MacDowell, A. A.; Balsara, N. P. Detection of subsurface structures underneath dendrites formed on cycled lithium metal electrodes. *Nat. Mater.* **2014**, *13*, 69–73.

[14] Steiger, J.; Kramer, D.; Mönig, R. Mechanisms of dendritic growth investigated by *in situ* light microscopy during electrodeposition and dissolution of lithium. *J. Power Sources* **2014**, *261*, 112–119.

[15] Cohen, Y. S.; Cohen, Y.; Aurbach, D. Micromorphological studies of lithium electrodes in alkyl carbonate solutions using *in situ* atomic force microscopy. *J. Phys. Chem. B* **2000**, *104*, 12282–12291.

[16] Aurbach, D.; Zinigrad, E.; Cohen, Y.; Teller, H. A short

review of failure mechanisms of lithium metal and lithiated graphite anodes in liquid electrolyte solutions. *Solid State Ionics* **2002**, *148*, 405–416.

[17] Qian, J. F.; Henderson, W. A.; Xu, W.; Bhattacharya, P.; Engelhard, M.; Borodin, O.; Zhang, J. G. High rate and stable cycling of lithium metal anode. *Nat. Commun.* **2015**, *6*, 6362.

[18] Qian, J. F.; Xu, W.; Bhattacharya, P.; Engelhard, M.; Henderson, W. A.; Zhang, Y. H.; Zhang, J.-G. Dendrite-free Li deposition using trace-amounts of water as an electrolyte additive. *Nano Energy* **2015**, *15*, 135–144.

[19] Zheng, G. Y.; Lee, S. W.; Liang, Z.; Lee, H. W.; Yan, K.; Yao, H. B.; Wang, H. T.; Li, W. Y.; Chu, S.; Cui, Y. Interconnected hollow carbon nanospheres for stable lithium metal anodes. *Nat. Nanotechnol.* **2014**, *9*, 618–623.

[20] Yan, K.; Lee, H. W.; Gao, T.; Zheng, G. Y.; Yao, H. B.; Wang, H. T.; Lu, Z. D.; Zhou, Y.; Liang, Z.; Liu, Z. F. et al. Ultrathin two-dimensional atomic crystals as stable interfacial layer for improvement of lithium metal anode. *Nano Lett.* **2014**, *14*, 6016–6022.

[21] Luo, W.; Zhou, L. H.; Fu, K.; Yang, Z.; Wan, J. Y.; Manno, M.; Yao, Y. G.; Zhu, H. L.; Yang, B.; Hu, L. B. A thermally conductive separator for stable Li metal anodes. *Nano Lett.* **2015**, *15*, 6149–6154.

[22] Cheng, X. B.; Hou, T. Z.; Zhang, R.; Peng, H. J.; Zhao, C. Z.; Huang, J. Q.; Zhang, Q. Dendrite-free lithium deposition induced by uniformly distributed lithium ions for efficient lithium metal batteries. *Adv. Mater.* **2016**, *28*, 2888–2895.

[23] Ji, X. L.; Liu, D.-Y.; Prendiville, D. G.; Zhang, Y. C.; Liu, X. N.; Stucky, G. D. Spatially heterogeneous carbon-fiber papers as surface dendrite-free current collectors for lithium deposition. *Nano Today* **2012**, *7*, 10–20.

[24] Yang, C. P.; Yin, Y. X.; Zhang, S. F.; Li, N. W.; Guo, Y. G. Accommodating lithium into 3D current collectors with a submicron skeleton towards long-life lithium metal anodes. *Nat. Commun.* **2015**, *6*, 8058.

[25] Liang, Z.; Zheng, G. Y.; Liu, C.; Liu, N.; Li, W. Y.; Yan, K.; Yao, H. B.; Hsu, P. C.; Chu, S.; Cui, Y. Polymer nanofiber-guided uniform lithium deposition for battery electrodes. *Nano Lett.* **2015**, *15*, 2910–2916.

[26] Cheng, X.-B.; Peng, H.-J.; Huang, J.-Q.; Zhang, R.; Zhao, C.-Z.; Zhang, Q. Dual-phase lithium metal anode containing a polysulfide-induced solid electrolyte interphase and nanostructured graphene framework for lithium–sulfur batteries. *ACS Nano* **2015**, *9*, 6373–6382.

[27] Ji, L. W.; Zhang, X. W. Fabrication of porous carbon nanofibers and their application as anode materials for rechargeable lithium-ion batteries. *Nanotechnology* **2009**, *20*, 155705.

[28] Ji, L. W.; Yao, Y. F.; Toprakci, O.; Lin, Z.; Liang, Y. Z.; Shi, Q.; Medford, A. J.; Millns, C. R.; Zhang, X. W. Fabrication of carbon nanofiber-driven electrodes from electrospun polyacrylonitrile/polypyrrole bicomponents for high-performance rechargeable lithium-ion batteries. *J. Power Sources* **2010**, *195*, 2050–2056.

[29] Cheng, X.-B.; Zhang, R.; Zhao, C.-Z.; Wei, F.; Zhang, J.-G.; Zhang, Q. A review of solid electrolyte interphases on lithium metal anode. *Adv. Sci.* **2016**, *3*, 1500213.

[30] Leroy, S.; Martinez, H.; Dedryvère, R.; Lemordant, D.; Gonbeau, D. Influence of the lithium salt nature over the surface film formation on a graphite electrode in Li-ion batteries: An XPS study. *Appl. Surf. Sci.* **2007**, *253*, 4895–4905.

[31] Xiong, S. Z.; Xie, K.; Diao, Y.; Hong, X. B. Characterization of the solid electrolyte interphase on lithium anode for preventing the shuttle mechanism in lithium–sulfur batteries. *J. of Power Sources* **2014**, *246*, 840–845.

[32] Nie, M. Y.; Lucht, B. L. Role of lithium salt on solid electrolyte interface (SEI) formation and structure in lithium ion batteries. *J. Electrochem. Soc.* **2014**, *161*, A1001–A1006.

[33] Kundu, S.; Wang, Y. M.; Xia, W.; Muhler, M. Thermal stability and reducibility of oxygen-containing functional groups on multiwalled carbon nanotube surfaces: A quantitative high-resolution XPS and TPD/TPR study. *J. Phys. Chem. C* **2008**, *112*, 16869–16878.

[34] Fong, R.; Von Sacken, U.; Dahn, J. R. Studies of lithium intercalation into carbons using nonaqueous electrochemical cells. *J. Electrochem. Soc.* **1990**, *137*, 2009–2013.

[35] Aurbach, D.; Daroux, M. L.; Faguy, P. W.; Yeager, E. Identification of surface films formed on lithium in propylene carbonate solutions. *J. Electrochem. Soc.* **1987**, *134*, 1611–1620.

[36] Aurbach, D.; Ein-Eli, Y.; Markovsky, B.; Zaban, A.; Luski, S.; Carmeli, Y.; Yamin, H. The study of electrolyte solutions based on ethylene and diethyl carbonates for rechargeable Li batteries II. Graphite electrodes. *J. Electrochem. Soc.* **1995**, *142*, 2882–2889.

[37] Miao, R. R.; Yang, J.; Feng, X. J.; Jia, H.; Wang, J. L.; Nuli, Y. Novel dual-salts electrolyte solution for dendrite-free lithium-metal based rechargeable batteries with high cycle reversibility. *J. Power Sources* **2014**, *271*, 291–297.

[38] Guo, J.; Wen, Z. Y.; Wu, M. F.; Jin, J.; Liu, Y. Vinylene carbonate–$LiNO_3$: A hybrid additive in carbonic ester electrolytes for SEI modification on Li metal anode. *Electrochem. Commun.* **2015**, *51*, 59–63.

[39] Xiong, S. Z.; Xie, K.; Diao, Y.; Hong, X. B. Properties of surface film on lithium anode with $LiNO_3$ as lithium salt in electrolyte solution for lithium–sulfur batteries. *Electrochim. Acta* **2012**, *83*, 78–86.